Supplementary Information

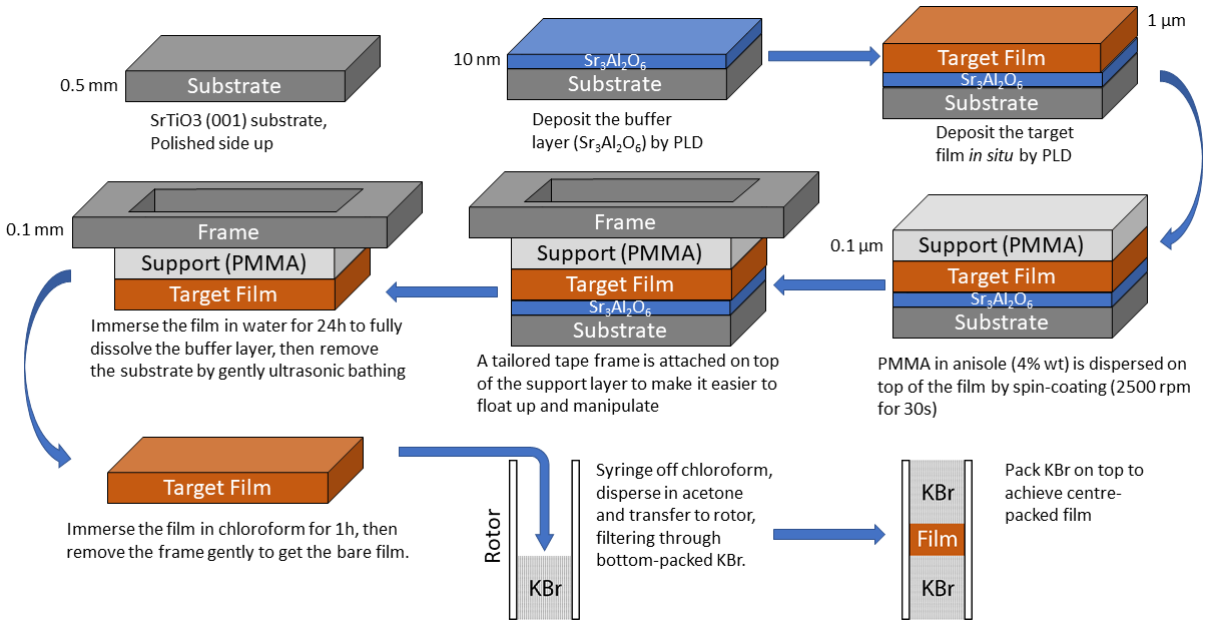

Figure S1: Schematic of the lift off and rotor packing procedure, including approximate thicknesses of the different layers.

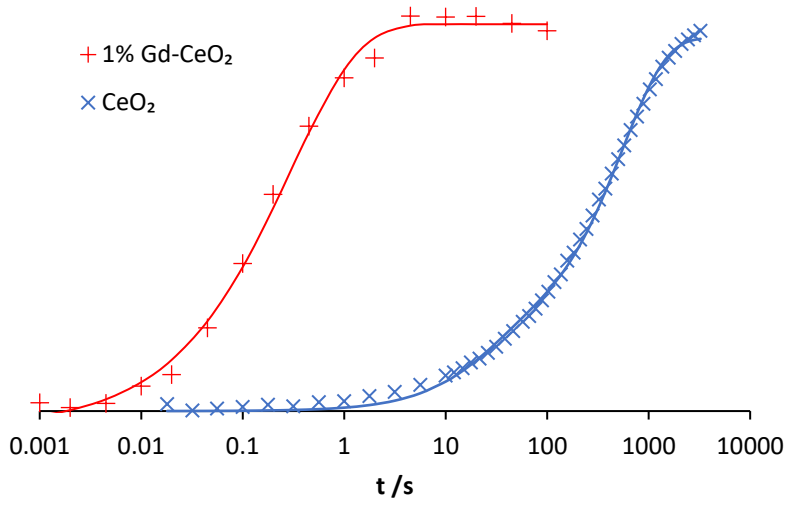

	CeO_2	Gd-CeO_2
T_1 /s	317	0.293
β	0.57	0.63

Figure S2: ^{17}O saturation recovery data for CeO_2 and 1 at% Gd doped CeO_2, as well as the fitted parameters from stretched exponential functions: $I = I_0\left[1 - \exp\left(-\left(\frac{t}{T_1}\right)^{\beta}\right)\right]$. A solid-state synthesis was used for the Gd-CeO_2 sample: Gd_2O_3 and CeO_2 were ground, pelletised and fired at 1500 °C for 48 h, before regrinding and refiring for a further 48 h.

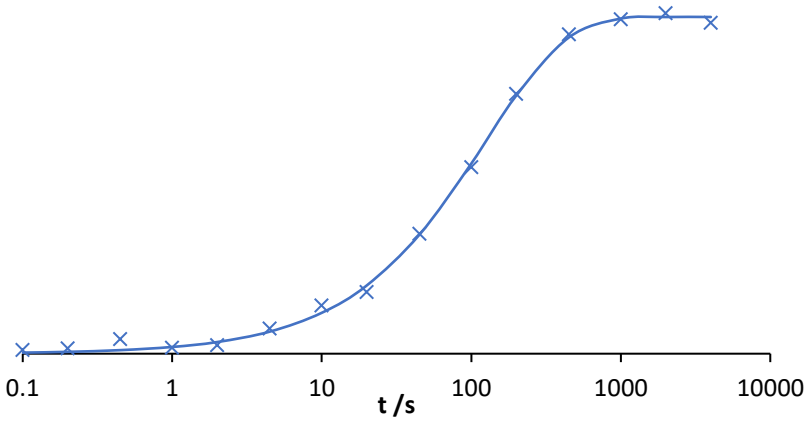

Figure S3: ^{17}O saturation recovery data for ^{17}O-enriched $SrTiO_3$, fitted to a stretched exponential function $I = I_0\left[1 - \exp\left(-\left(\frac{t}{T_1}\right)^{\beta}\right)\right]$ with T_1 = 126 s and β = 0.81.

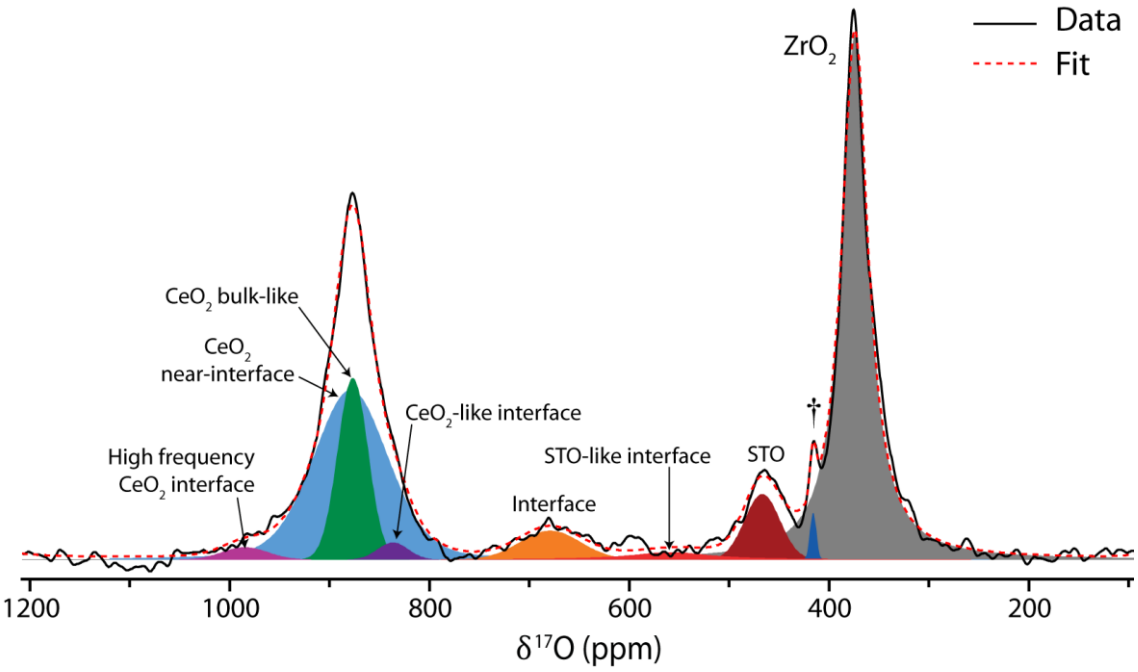

Figure S4: ^{17}O NMR spectrum of a second batch of 4× CeO_2–STO nanopillar lift-off films enriched at 450 °C, recorded at 9.40 T and 50 kHz MAS using a Hahn echo pulse sequence, a 0.1 s recycle delay and 4.2 million scans (5 days). The signal marked with a † is tentatively assigned to a minor component of the ZrO_2 rotor with a local dopant/impurity.

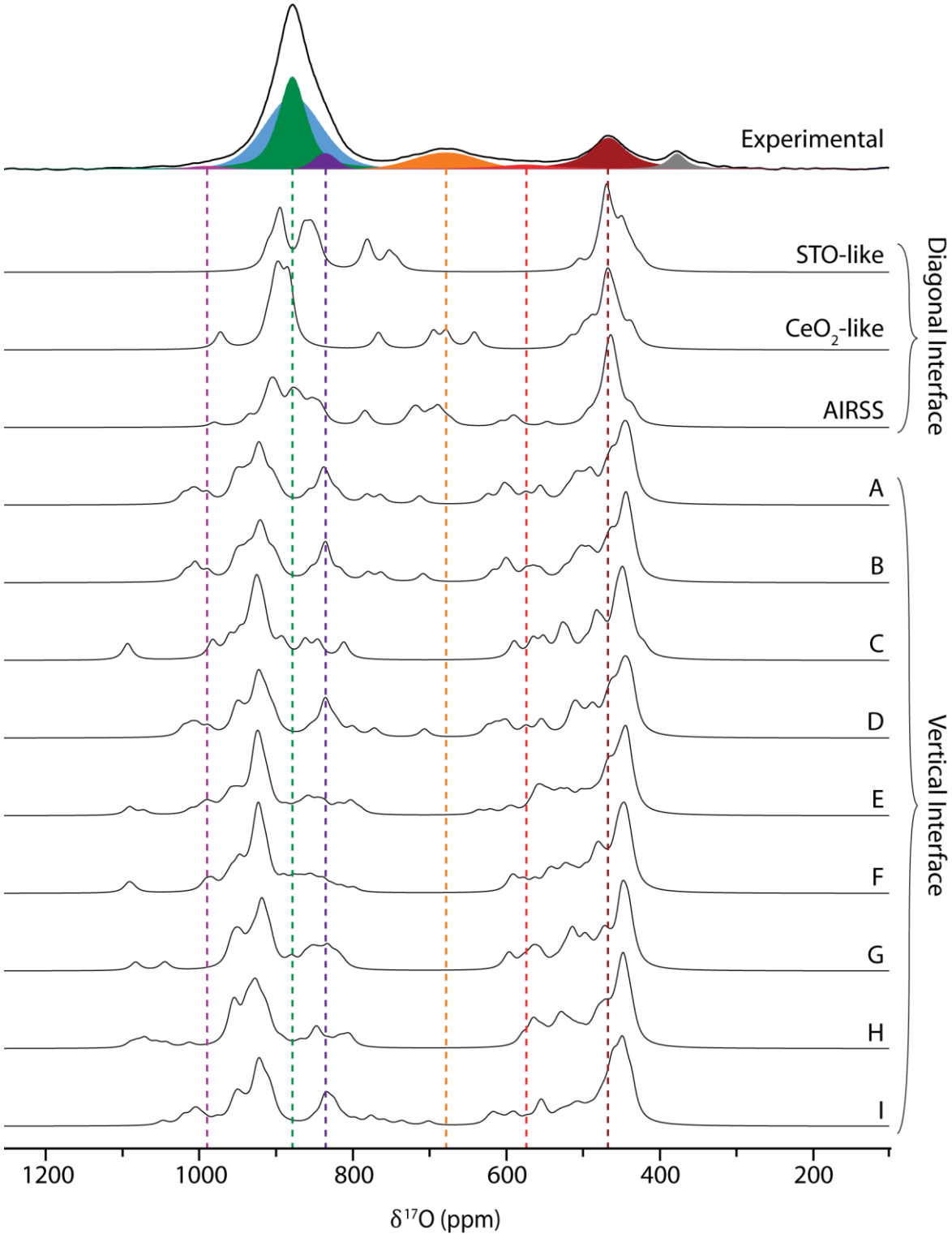

Figure S5: Simulated interface spectra created by inserting a Lorentzian peak with a FWHM of 15 ppm at the calculated ^{17}O shift for each environment within ±6 Å of the interface for each of the calculated structures.

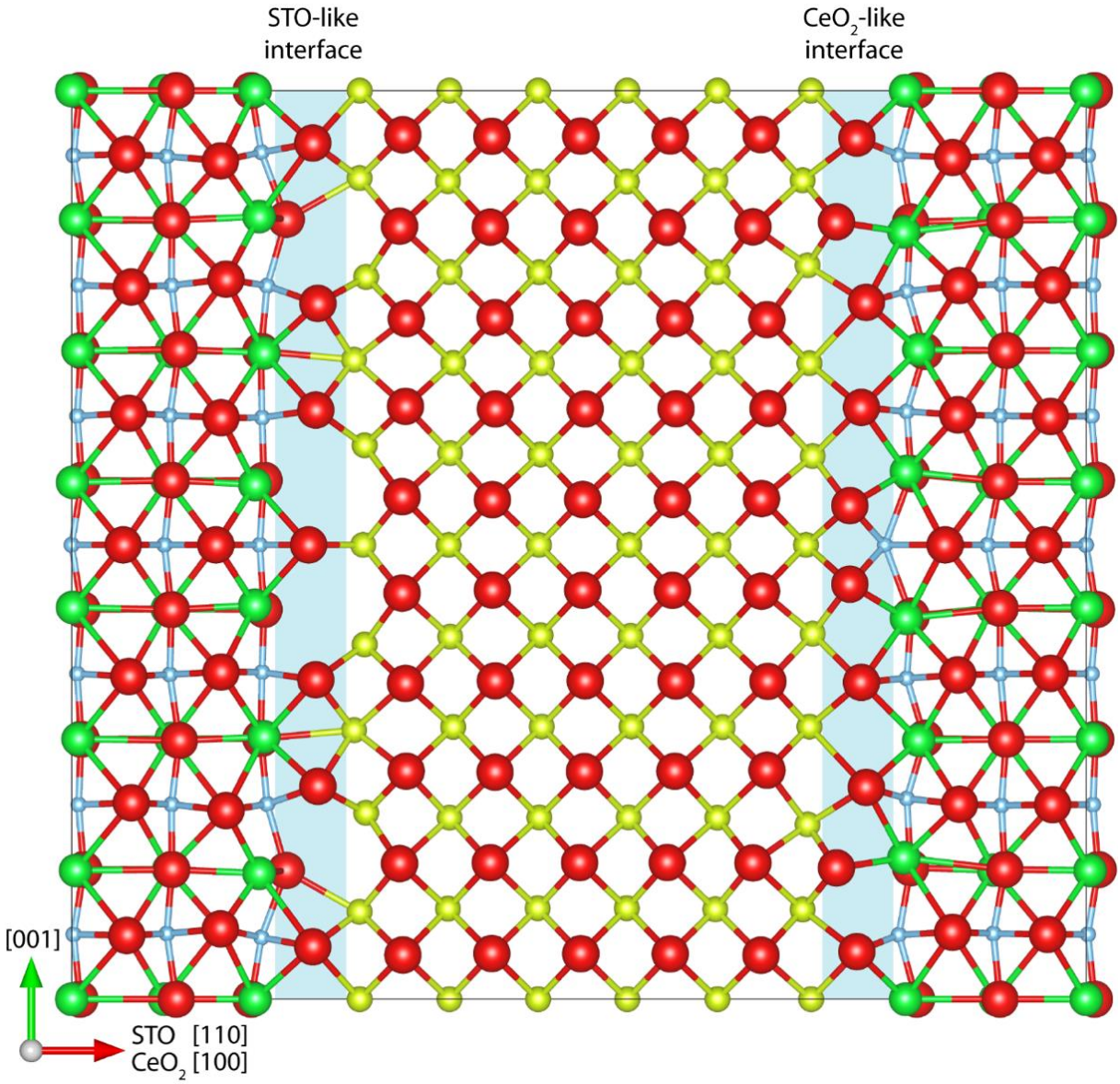

Figure S6: The simple model for the 45° CeO_2–STO interface, showing the CeO_2-like interface with 20 O^{2-} ions and the STO-like interface with 14 O^{2-} ions. The ions are coloured as follows: O – red, Sr – green, Ti – blue, Ce – yellow.

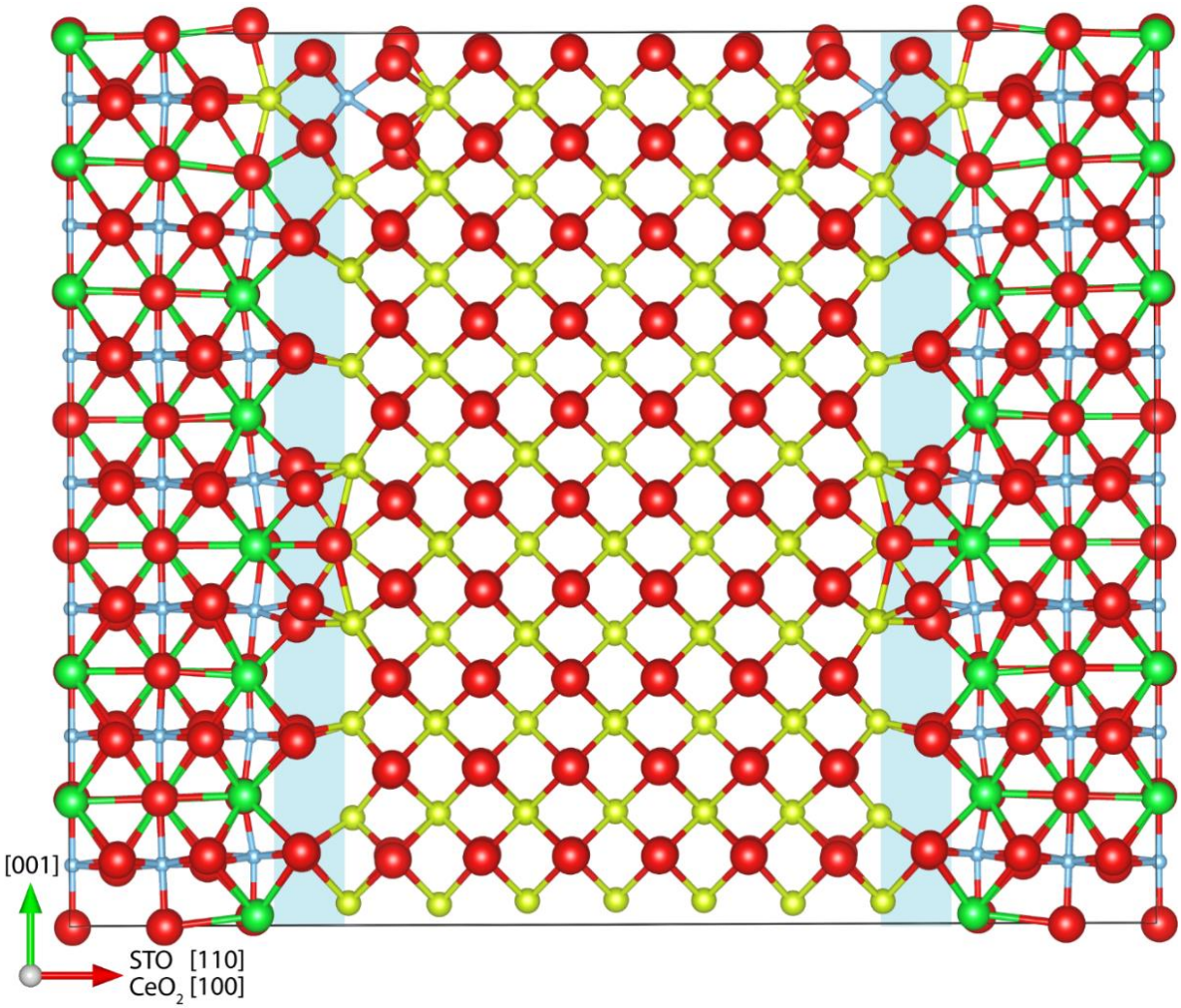

Figure S7: The model for the 45° interface found from random structure searching, showing two equivalent interfaces each with 17 O^{2-} ions. The ions are coloured as follows: O – red, Sr – green, Ti – blue, Ce – yellow.

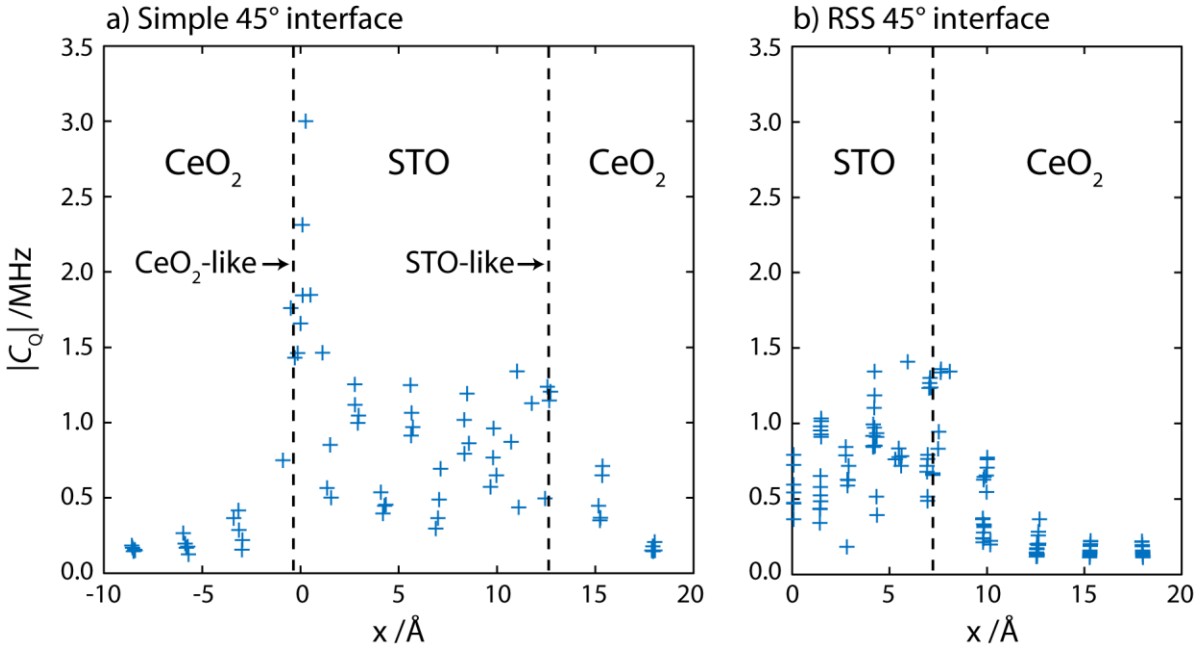

Figure S8: Calculated absolute quadrupolar coupling constants ($|C_Q|$) as a function of distance for the ^{17}O environments in the two models for the 45° interface. The interfaces are marked with dashed lines.

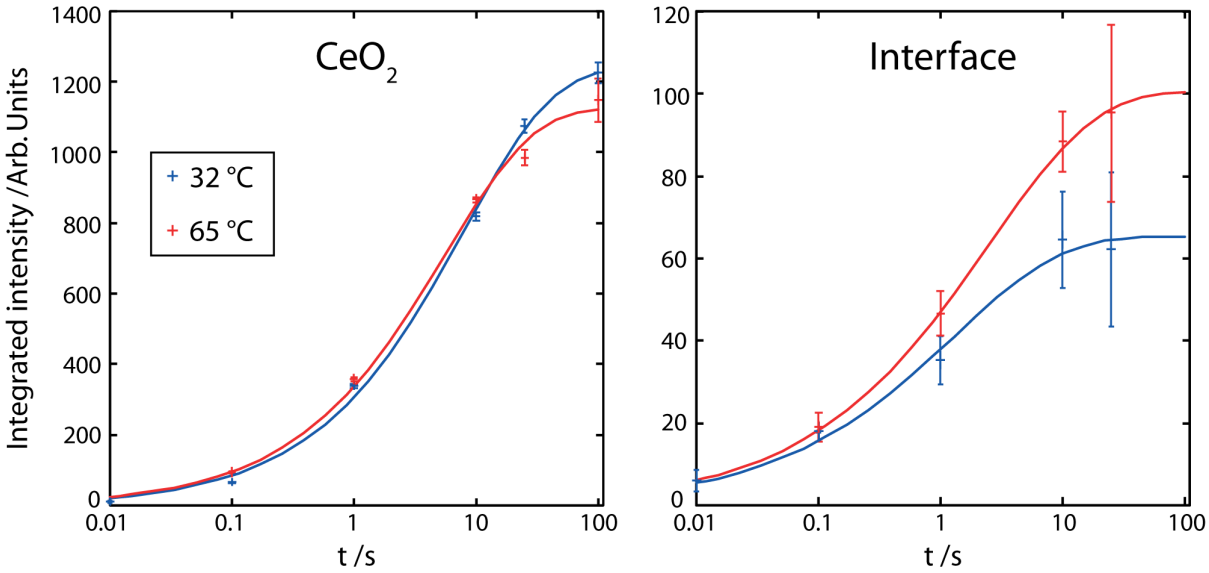

Figure S9: Saturation recovery data for the CeO_2 and 45° interface ^{17}O NMR signals for CeO_2:STO lift-off films enriched at 250 °C, recorded at 40 kHz. A variable number of scans was used for each time point to achieve significant signal-to-noise ratios in as little time as possible; a total experimental time of 140 hours was still required at each temperature point. The error bars were determined from the noise floor for each time step. The data are fitted to stretched exponential functions: $I = I_0\left[1 - \exp\left(-\left(\frac{t}{T_1}\right)^{\beta}\right)\right]$, with the stretching exponent β = 0.55 and 0.5 for the CeO_2 and interface signals respectively, and the spin-lattice relaxation T_1 constants in Table S1.

Table S1: Fitted T_1 constants for the CeO_2 and 45° interface ^{17}O NMR signals for CeO_2:STO lift-off films enriched at 250 °C. Given the error in the measured intensities for the interface signal, there is a significant error in the fitted T_1 constants; this error is multiplicative rather than additive, so the positive and negative error bars are not equal and the possible T_1 constants are instead given by a range.

	T_1 /s	
T /°C	CeO_2	Interface
32	8.1 ± 0.5	0.6 – 3.8
65	5.4 ± 0.4	0.9 – 2.6

Table S2: On-the-fly generation (OTFG) settings for the soft psuedopotential set (QC5).

Element	OTFG string
O	2|1.7|12|13|15|20:21(qc=5)
Ce	2|2.2|7|7|9|50U:60:51:43:52L(qc=5)
Sr	3|2.0|7|7|9|40U:50:41:42(qc=5)
Ti	3|1.9|8|9|10|30U:40:31:32(qc=5)

Table S3: On-the-fly generation (OTFG) settings for the standard pseudopotential set (CASTEP C18).

Element	OTFG string
O	2|1.1|17|20|23|20:21(qc=8)
Ce	2|2.1|9|10|11|50U:60:51:43:52L(qc=6)
Sr	3|2.0|5|6|7|40U:50:41:42
Ti	3|1.8|9|10|11|30U:40:31:32(qc=5.5)

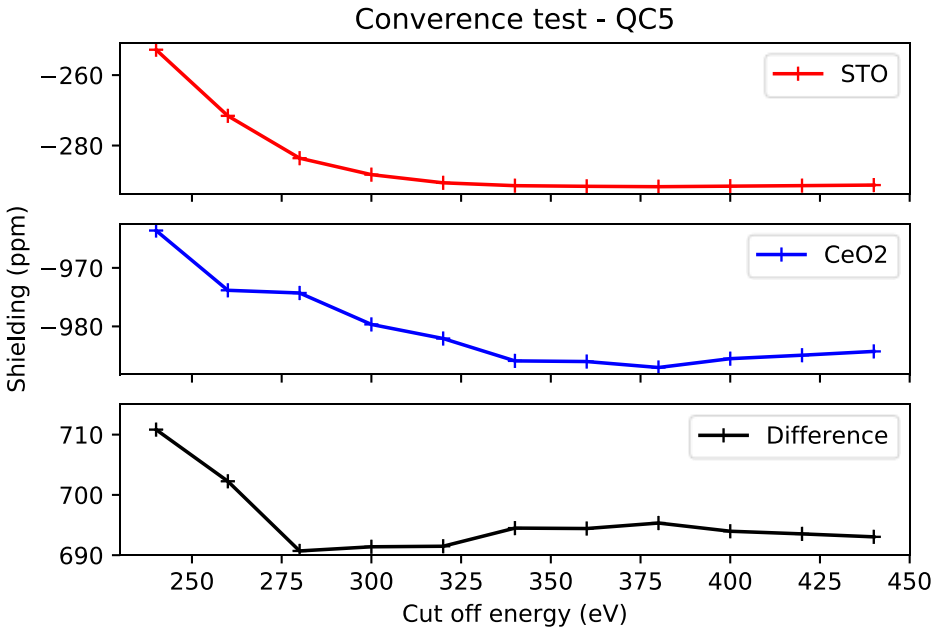

Figure S10: Convergence test of calculated ^{17}O shieldings for pure CeO_2 and STO with increasing plane wave cut off energies using the soft variants of the pseudopotentials as provided in the QC5 library. A cut off energy of 350 eV is found to be sufficient.

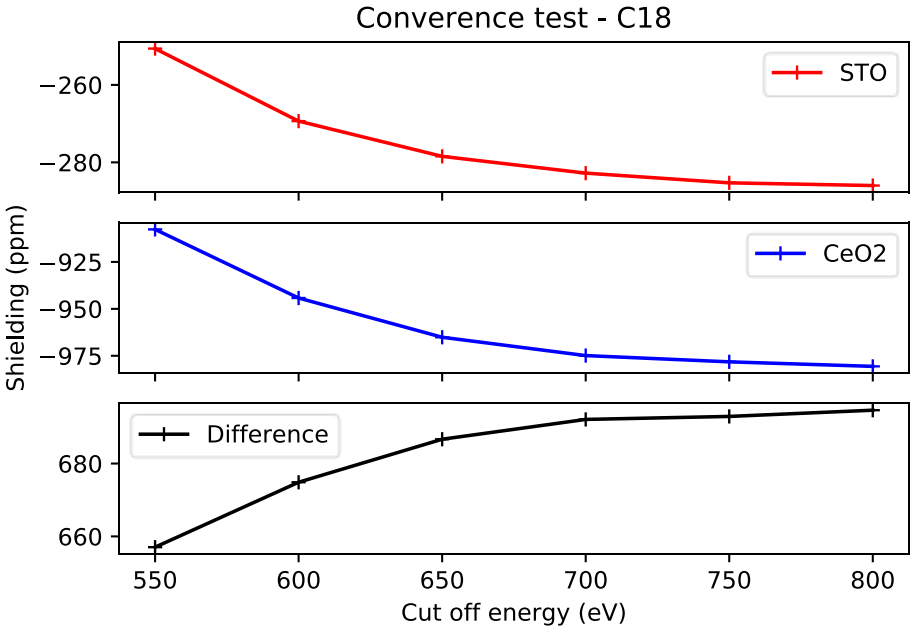

Figure S11: Convergence test of calculated ^{17}O shieldings for pure CeO_2 and STO with increasing plane wave cut off energies using the standard pseudopotentials set as provided in the C18 library. A cut off energy of 700 eV is found to be sufficient for obtaining a converged shielding difference.

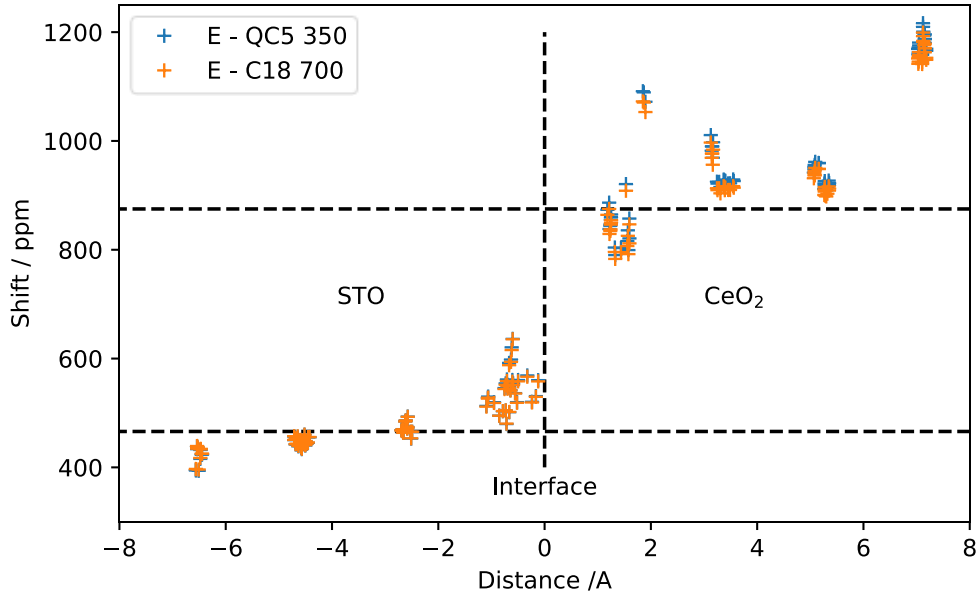

Figure S12: Comparison of the calculated shifts for one of the models for the 0° interface (E) computed using the soft QC5 and standard C18 pseudopotential sets. The shift values are almost identical for STO, and for CeO_2 there is an approximately 15 ppm discrepancy, which is not significant compared to the dispersion of shifts and the experimental linewidths.

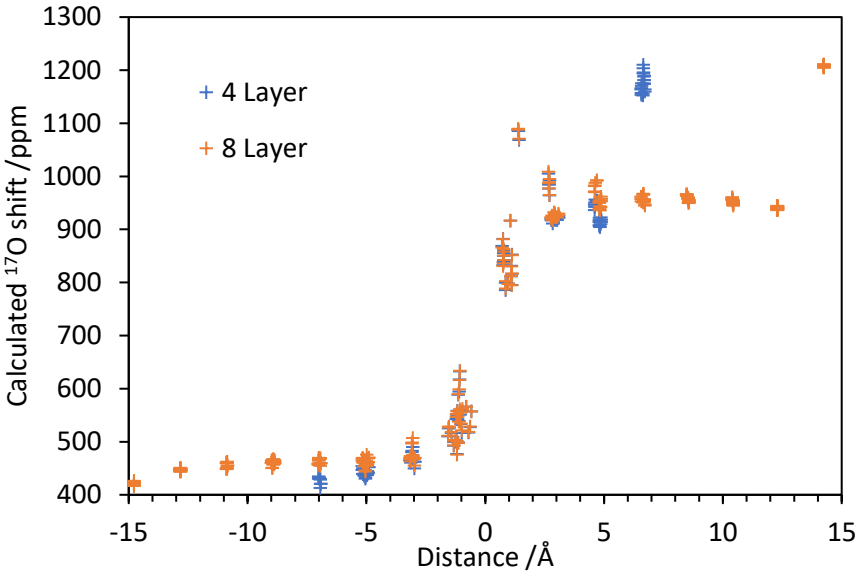

Figure S13: Comparison of the calculated ^{17}O shifts as a function of distance from the interface for 4- and 8-layer models of structure E for the 0° interface. As can be seen, the calculated shifts for the first two oxide layers on either side of the interface are almost indistinguishable for the two models, indicating that the 4-layer model is sufficient to converge these shifts.

Supplementary Note 1

Quantification of CeO_2–STO VAN Facets

To quantify the proportions of the different types of interface in the CeO_2–STO VAN films, the STEM image in Figure 1a in the main text was analysed using the Directionality plugin for the ImageJ software.[1] First, the edges were identified by applying a Gaussian blur to obscure the atomic resolution before setting an appropriate threshold (Figure S14a). The directions of the edges were then analysed using the local gradient orientation method (determined from a 5×5 Sobel filter); the histogram of orientations is shown in Figure S14b.

This analysis clearly identifies the 0° and 45° interfaces, in a ratio of ~3:1. The remaining orientations correspond to the rounding of the edges observed in the STEM image, although there is some clustering around ~20° and ~70°. This rounding could be due to poorly defined or high index interfaces, but could also arise from 0° or 45° interfaces with steps, or from blurring of the STEM image when the interface is not uniform throughout thickness of the film, since the image represents a vertical projection.

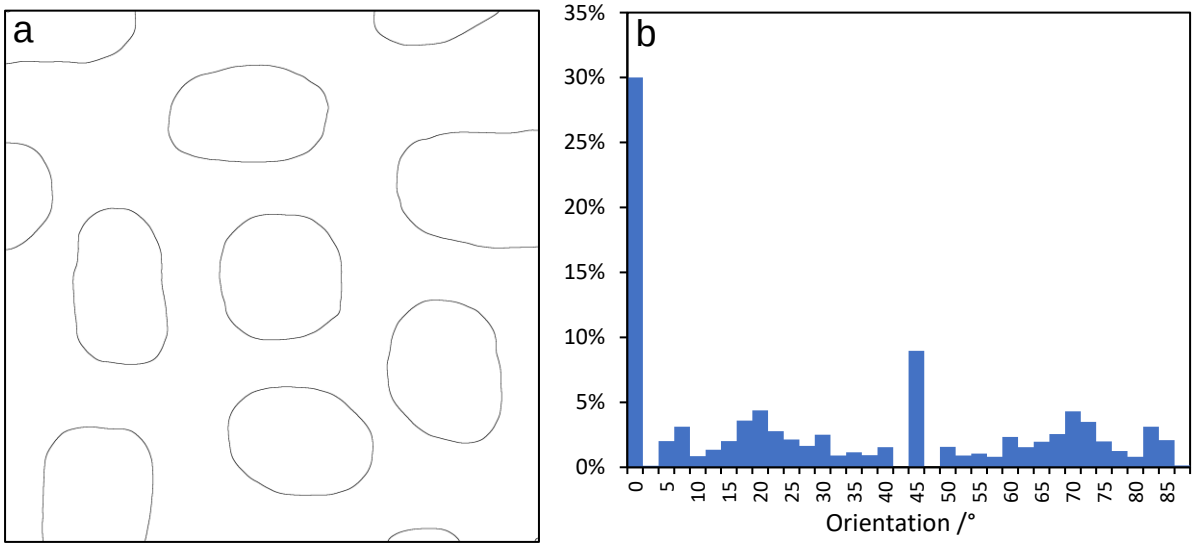

Figure S14: a) The edges extracted from Figure 1a in the main text, the STEM image reproduced from Zhu et al.[2] of a 20 at% Sm-doped-CeO_2–STO VAN film. b) The corresponding histogram of orientations as determined by the local gradient orientation method in the ImageJ Directionality software, using bins of 2.5° and folding the orientations at 90–180° onto 0–90°.

Supplementary Note 2

Exchange-induced Spin–Spin (T_2) decay

To investigate the effect of exchange on T_2 relaxation, simulations of Hahn echo experiments for a simple model of two-site exchange were performed using the MATLAB software, similar to Zhou et al.'s previous simulations.[3] Although there are clearly more than two possible environments for the oxygen ions at the interface, a two-site model is sufficient to explore the effect that motion has on transverse relaxation when it is on a comparable timescale to the range of frequencies for the different environments being sampled.

2048 spins were considered, half of which at time zero were in site A and the other half in site B. At each time step, a relative phase difference was developed between spins in sites A and B, given by the frequency separation of the sites; jumps or exchange between sites were then allowed where the probability of exchanging site is given by the product of the timestep and the jump frequency. For the first half of the echo the relative phase developed was positive, then for the second half of the echo the relative phase developed was negative. At the echo top, the vector sum of all the spins was calculated, which is proportional to the observed intensity in the Fourier transformed spectrum. This process was then repeated for different lengths of echo to produce a T_2 decay curve. The T_2 constant was extracted by fitting to the function:

$$I = I_0 \exp\left[-\left(\frac{t}{T_2}\right)^{\beta}\right], \tag{S1}$$

where t is the total echo length and β is the stretching exponent. This procedure was repeated for different jump frequencies and site separation frequencies to yield the data in Figure S15.

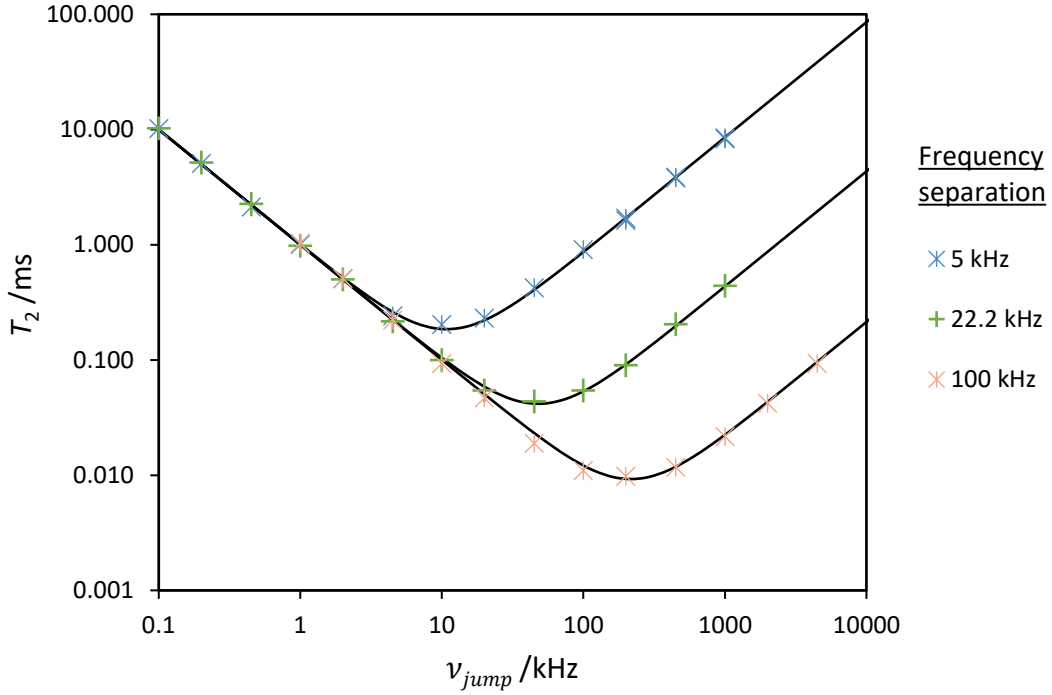

Figure S15: Simulated T_2 constants as a function of jump rate (ν_{jump}), for two site exchange of sites separated by different frequencies. The black lines are given by equation (S2).

On a log–log plot, typical V-shaped curves are seen, with a T_2 minimum when the jump rate is on the order of the frequency separation of the sites. The data can be reproduced by equation (S2):

$$T_2 = \frac{1 + \frac{2}{\pi^2}\left(\frac{\nu_{\mathrm{jump}}}{\nu_{\mathrm{sep}}}\right)^2}{\nu_{\mathrm{jump}}} \qquad \text{(S2)}$$

where ν_{jump} is the jump frequency and ν_{sep} is the frequency separation of the sites. Differentiation yields the T_2 minimum when $\nu_{\mathrm{jump}} = \frac{\pi}{\sqrt{2}}\nu_{\mathrm{sep}} = 2.22\,\nu_{\mathrm{sep}}$.

In the fast exchange limit $\nu_{\mathrm{jump}} \gg \nu_{\mathrm{sep}}$, $T_2 = 2\nu_{\mathrm{jump}}/(\pi^2\nu_{\mathrm{sep}}^2)$. This is the same as the expression given by Bain for the fast exchange contribution to T_2:[4] $T_2 = 2k/\delta^2$, with $k = \nu_{\mathrm{sep}}$ and noting that δ is half the frequency separation in rad s^{-1}, so $\nu_{\mathrm{jump}} = 2 * (\delta/2\pi)$.

We note that in the fitting of the T_2 decay curves, β took the expected value of ~1 except in the vicinity of the T_2 minimum where it increased to around 2: this corresponds to a more precipitous decrease in signal than for an exponential decay (see Figure S16 and Table S4).

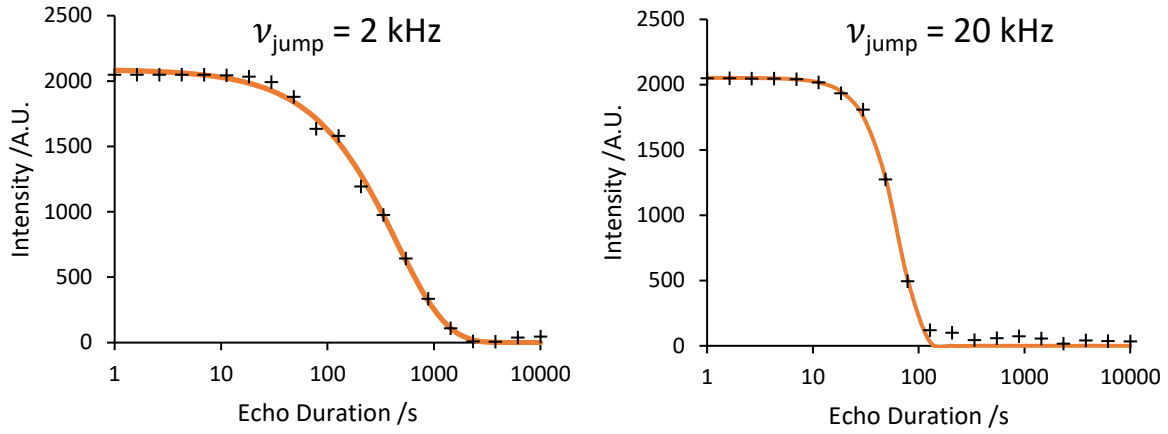

Figure S16: Representative simulated and fitted T_2 decay curves for two different jump rates and ν_{sep} = 15 kHz. The fitting parameters are given in Table S4.

Table S4: Fittings parameters for the T_2 decay curves in Figure S16.

	ν_{jump} / kHz	
	2	20
T_2 /ms	0.446	0.0679
β	0.93	2.26

References

(1) Tinevez, J.-Y. Directionality - ImageJ https://imagej.net/Directionality (accessed Jul 27, 2020).

(2) Zhu, B.; Schusteritsch, G.; Lu, P.; MacManus-Driscoll, J. L.; Pickard, C. J. Determining Interface Structures in Vertically Aligned Nanocomposite Films. *APL Mater*. **2019**, *7* (6), 061105.

(3) Zhou, L.; Leskes, M.; Liu, T.; Grey, C. P. Probing Dynamic Processes in Lithium-Ion Batteries by in Situ NMR Spectroscopy: Application to $Li_{1.08}Mn_{1.92}O_4$ Electrodes. *Angew. Chemie - Int. Ed.* **2015**, *54* (49), 14782–14786.

(4) Bain, A. D. Chemical Exchange in NMR. *Prog. Nucl. Magn. Reson. Spectrosc.* **2003**, *43* (3–4), 63–103.